Authors' Response for Revision_02
Preprint: https://egusphere.copernicus.org/preprints/2025/egusphere-2025-1977/)

We thank the editor and the anonymous referee for giving us further opportunity to strengthen our manuscript through valuable feedback. We have carefully addressed all comments, suggestions, and concerns and made thorough revisions. The revisions include additional analyses, rewriting, and clearer explanations. We believe those revisions have significantly improved the accuracy of our findings, presentations and the overall readability of the manuscript. Thank you for your support during the revision process.

RC: Referee Comment (in blue font)
AAR: All Authors' Responses (in black regular font)
The modified texts in the revised manuscript are in *black italics.*

Detailed Response to Referee #1

RC: 1. Use of observations and construction of the Jacobian. The manuscript still does not clearly explain how the observations are used in the inversion. The authors' response suggests that observations are grouped by political state when constructing the Jacobian. This raises the concern that each state may be constrained only by observations within that same state. This would be some form of extreme localization, which is not needed in analytical inversions. This point must be clarified unambiguously. If the inversion is indeed structured in this way, the methodology must be revised.

AAR: Thank you for your comment. We apologize for the ambiguous statements in the revised version. To effectively address the above concern, we have taken the following steps: 1) a comprehensive rewrite of the concerned methodological part, and 2) a better explanation of the inversion approach employed within the context of our study. We have revised the manuscript to enhance clarity in both our statements and equations.

Our clarifications are as follows: The inversion focuses on capturing near-field influence on observations, minimising the overinterpretation of far-field influences by assigning minimal weight to far-field signals. The Jacobian matrix must thus be designed with elements that represent the response in mixing ratios to the state vectors, controlled by each scaling factor. Here, the state vectors correspond to the total emission in each political state. The derivation of the Jacobian matrix elements in the present study follows nearly the method adopted by Pillai et al. (2016) (see Section 3.2 in their study), Ye et al. (2020) (see Section 2.6 in their study), and

Kuhlmann et al. (2020) (see Section 3.1 in their study). Importantly, mixing ratio simulations are not artificially truncated at state boundaries, so the Jacobian naturally captures cross-state sensitivities when transport is applied freely across the model domain, as in our study. Similar targeted approaches are widely applied in other studies, such as Bisht et al., 2023; Pendergrass et al., 2025; Kumar et al., 2022; Bruch et al., 2025; and Pillai et al., 2016, and demonstrated the benefits in inferring targeted fluxes. The concept is also illustrated in Broquet et al. (2018) (see Section 2.5 of their study). For instance, Bisht et al. (2023) implemented a localised methane inversion in which observations influence only nearby state-vector elements within a defined localised radius, explicitly demonstrating improved stability and realism of inferred fluxes. Pendergrass et al. (2025) apply explicit spatial localisation when assimilating TROPOMI methane observations, showing that restricting long-range influence is essential for robust inverse-based estimations. At finer scales, Kumar et al. (2022) demonstrate that methane inversions targeting localised emission sources must rely on near-field observational sensitivity to avoid ill-posed solutions. Bruch et al. (2025) employ regional scaling factors in an ensemble-based inversion framework, where observations predominantly constrain geographically proximate emission regions through transport sensitivities.

Acknowledging the reported ambiguity in statements, we revised the methodology section.

Revised Lines: 210-228 as follows:

"Here, **K** *is the m x n Jacobian matrix, representing the sensitivity of the mixing ratio simulated by the forward model to the state vector. The elements of* **K** *are thus:* $k_{m,n} = \frac{\partial F_m(x)}{\partial x_n}$

Since we have not implemented the adjoint model for our forward transport model, the Jacobian matrix is constructed using a finite-difference approach: the transport model (WRF-GHG) is applied to perturbed emissions, and sensitivities of the resulting mixing ratio simulations are derived. This perturbation-based Jacobian construction is mathematically equivalent to computing the response functions to state vectors. The Jacobian matrix in the present study ensures capturing near-field influence on observations and minimizes the over-interpretation of far-field influences. For robust flux estimations at regional and sub-regional scales, the importance of relying more on near-field sensitivity is widely accepted, and such inverse applications have demonstrated their potential to minimize ill-posed solutions in finer scales (e.g. Pendergrass et al., 2025; Bruch et al., 2025; Bisht et al., 2023; Kumar et al., 2022; and Broquet et al., 2018).

The elements in the Jacobian matrix are derived as follows:

$$k_{m,n} = \frac{(Y_{pert})_m - Y_m}{(\phi_{pert})_n - \phi_n}$$

The above derivation closely follows methods implemented in Pillai et al. (2016), Ye et al. (2020), and Kuhlmann et al. (2020). Here, Υ and Υ_{pert} are the 1-D representations of the column mixing ratio and the perturbed column mixing ratio, respectively, both derived by our forward model, corresponding to each m elements in the measurement vector $\mathbf{y}$. *ϕ and ϕ_{pert} represent emissions and perturbed emissions, respectively, corresponding to each n elements in the state vector* $\boldsymbol{x}$. *Note that perturbed mixing ratios are simulated by applying the transport operator (WRF-GHG) to perturbed emissions, as explained before. By our design, the elements in the* $\boldsymbol{y}$ *correspond to the available column mixing ratio observations over a month at 0.1° x 0.1° spatial resolution, and the elements in the* $\boldsymbol{x}$ *refer to total monthly emissions of each political state."*

RC: 2. Insufficient presentation of inversion results. Only national annual total emissions are shown in the manuscript. Even though the appendix now includes prior and posterior values for five larger regions, a spatially resolved plot of posterior adjustments at the political-state level (i.e., for each element of the state vector) is essential. Without such a figure, it is impossible to assess whether the inversion leads to reasonable spatial adjustments. In addition, no statistics are presented that quantify model–observation agreement in the prior and posterior. Such diagnostics are fundamental to evaluating the credibility of the inversion. Without these results, it is not possible to evaluate or trust the posterior emission estimates.

AAR: In response to the above comment regarding statistics, we have included quantitative prior–posterior model-observation agreement statistics in the revised manuscript (new Fig. 10, providing diagnostic metrics is added to the main manuscript). These diagnostics indicate improved consistency between simulations and observations after inversion. For example, the distributions of mean biases and RMSEs become narrower after inversion, and the residual probability density functions are more centred around zero. R^2 values are higher after inversion than before. (see Fig. 10).

Also, we have provided state-wise and regional-wise flux adjustment details and included Fig. S13 in the revised version.

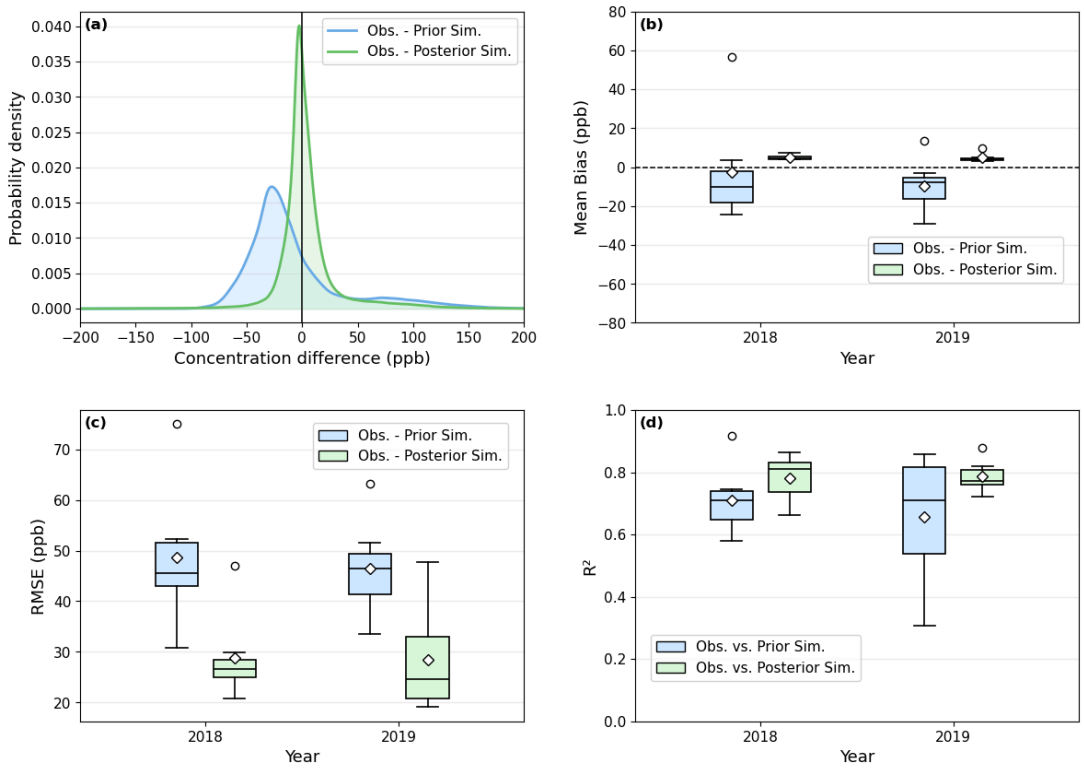

Figure 10: Model-Observation mismatches before and after optimization: (a) Probability density for difference between observed (Obs.) and simulated (Sim.) concentrations, (b) monthly Mean Bias, (c) monthly RMSE and (d) R^2 between observations and simulations before (blue) and after (green) optimization. In the legend, the terms Prior Sim. and Post Sim refer to simulations before and after optimization, respectively.

Revised Lines: 438-442 as follows:

"The model-observation mismatches before and after optimization are shown in Fig. 10. The optimization significantly reduces mismatches in XCH_4 as expected for a robust inversion, resulting in a narrower distribution around zero. For example, in January 2018, the mean XCH_4 bias improves from -12.4 ppb (before optimization) to 5.2 ppb (after optimization). Simultaneously, the improved explanation of variance in statistics is found, indicating a better fit to the observed data after optimization (see Fig. 10).

Revised Lines: 472-475 as follows:

"Although our primary emphasis is on national-scale inversion estimates, the inversion framework explicitly resolves emissions at the state level, with each political state constituting an element of the state vector. The spatial distribution of flux adjustments is shown in Fig. S13, which illustrates how the inversion adjusts emissions across the states. Quantitative assessments of prior and posterior estimates are also presented region-wise in Fig. S13."

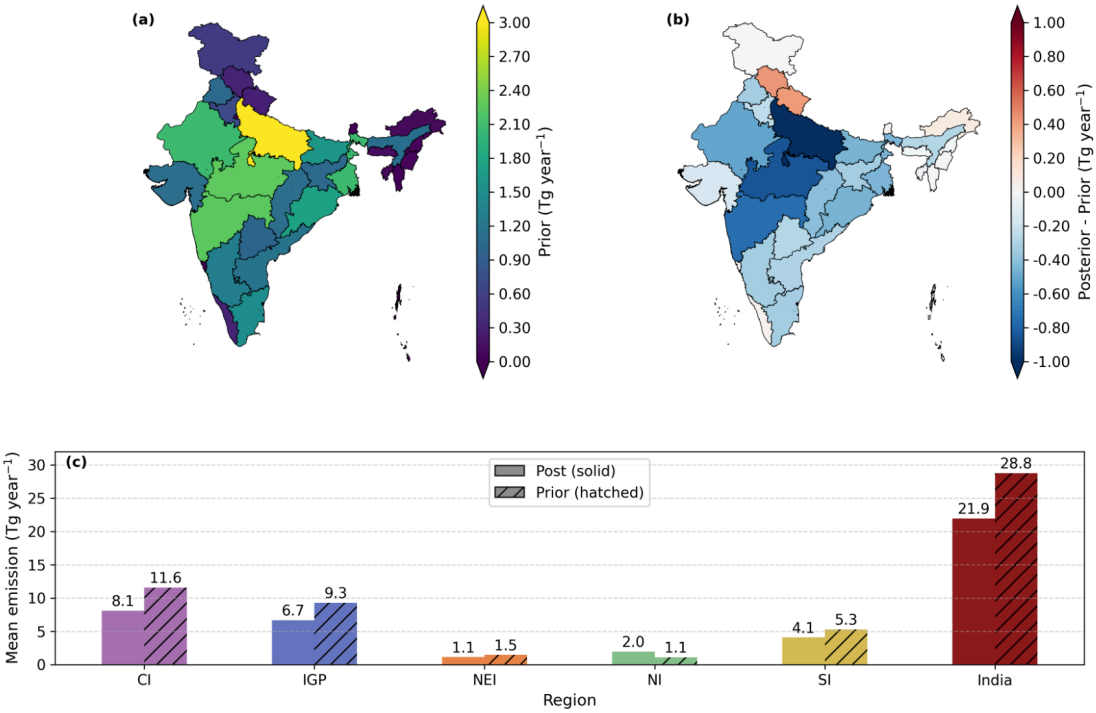

Figure S13: State-wise anthropogenic (a) prior and (b) flux adjustment (posterior minus prior) and (c) region-wise annual prior and posterior emission fluxes averaged for 2019.

RC: 3. Explanations of Equation (4). The motivation, derivation, and interpretation of Eq. (4) remain unclear. It is not explained why perturbations are used instead of defining a tracer per state, nor why a summation over states appears in this formulation. This equation must be clearly and transparently explained.

AAR: Please see our comment above regarding the rewrite of the methodological part and Eq. 4.

Revised Eq. 4 is now as follows:

$$k_{m,n} = \frac{(\Upsilon_{pert})_m - \Upsilon_m}{(\phi_{pert})_n - \phi_n}$$

Also, please refer to Lines 210-228 in the revised manuscript.

RC: 4. Model initialization and treatment of the CH_4 fields. The simulations are reinitialized daily with ERA5 and a 6-hour spin-up. It remains unclear whether the CH_4 fields are also reinitialized each day. If so, only emissions from the current day could be used to constrain emissions, which would strongly reduce the inversion's capability. Furthermore, the manuscript states that CAMS fields are corrected by a monthly factor of 1–3%, but the method for applying these corrections is not described. Both the CH_4 initialization procedure and the implementation of the CAMS corrections must be explicitly explained.

AAR: The CH_4 tracer fields are not reinitialized daily. Only meteorological fields are reinitialized daily using ERA5, followed by a 6-hour spin-up. The CH_4 mixing ratios are initialized with CAMS only on the first day of the simulation, and carried forward continuously to the following days.

For the background (CAMS) correction, the scaling factor is applied uniformly across the domain to the CH_4 background, specific for each month (i.e., one scaling factor per month). These monthly background scaling factors range from 1% to 3%.

We have revised the manuscript to better explain both the CH_4 re-initialization strategy and the background correction.

Revised Lines: 125-129 are as follows:

"Meteorological fields are reinitialized daily using ERA5 reanalysis, followed by a 6-hour spin-up period. In contrast, note that CH_4 tracer fields are initialized only at the beginning of the simulation and the simulated background fields are continuously transported across successive simulation days (i.e. not reintialized daily). This approach ensures that methane concentrations reflect the cumulative influence of emissions, preserving the temporal memory for inverse optimization of local surface fluxes."

Revised Lines: 133-137 are as follows:

"We have also considered the reported level of uncertainties in CAMS-simulated mixing ratios (e.g. Agustí-Panareda et al. (2023); Wang et al. (2023)) and applied a monthly scaling factor correction to our methane background (initialized by CAMS) to minimize the unrealistic representation of background contribution to methane mixing ratios. The scaling factor is applied uniformly across the domain to the CH_4 background, specific for each month (i.e., one scaling factor per month). These monthly background scaling factors range from 1% to 3%."

RC: 5. Abandonment of the stratospheric extension. The absence of a stratospheric extension introduces a systematic offset of 2–3% in the CH_4 columns, this cannot simply be ignored. This issue must be addressed.

AAR: We appreciate the above comment and included explicit statements in the revised version to avoid confusion. We agree that our model does not fully represent the whole atmosphere. However, the model profile is extended above the model top (~50 hPa) using satellite a-priori profiles, ensuring the same sampled air column corresponding to the observation datasets, also following a priori profile weights when computing the column-averaged mole fraction (see Sect. 2.4). Here, the assumption when extending the model top is that the model biases for the remaining stratospheric layer are small compared to that of the tropospheric counterpart (e.g. Wang et al., 2017). We have revised the manuscript by including a discussion of these aspects and point out that a complete treatment of the full atmosphere in the forward model may further reduce model uncertainties, while this limitation exists in the current study.

The manuscript is revised accordingly.

Revised Lines: 161-177 are as follows:

"The model top is set near ~50 hPa. When computing the column-averaged mole fractions from simulations, the model profile is extended above the model top utilizing satellite a priori profiles, ensuring the same sampled air column corresponding to the observation datasets, also following a priori profile weights when computing the column-averaged mole fraction (more details below). Here, we assume negligible model biases for the remaining atmospheric contribution above the model top compared to that of the tropospheric and lower stratospheric counterparts. Previous studies of stratospheric and tropospheric contributions to total column CH_4 demonstrated that the model biases in the stratospheric partial column tend to be smaller than those in the tropospheric partial column owing to the substantially higher tropospheric CH_4 contribution to the total column than stratospheric CH_4 (Wang et al., 2017). However, the assumption underlying the extension above the actual model top is a simplification of real-case conditions and may be considered when analyzing the results.

In the present study, the model simulations have not accounted for any impacts of stratospheric CH_4 chemistry reactions on mixing ratios. Ignoring chemical reactions is typically a valid assumption when considering the regional model domain and the considerably longer atmospheric lifetimes of target species, approximately 10 years for CH_4, than the simulation period. Excluding the OH reactions has shown a negligible impact on annual CH_4 at the regional scale, resulting in smaller biases than the measurement uncertainties (1 ppb for in situ measurements and 6 ppb for TCCON) and the typical magnitudes of the observational bias in the inversion (Callewaert et al., 2025). However, atmospheric CH_4 is susceptible to chemical reactions in the stratosphere, which warrants consideration in modelling and analyzing long time series such as decadal contributions."

RC: 6. Very coarse spatial resolution of the state vector. The state vector consists of only 36 political regions, which is extremely coarse for a country the size of India. Even with an analytical inversion, higher state-vector dimensionality are easily possible. Higher-resolution inversions using TROPOMI data have been demonstrated in the literature (e.g. https://egusphere.copernicus.org/preprints/2025/egusphere-2025-2622/). There is more spatial information in TROPOMI data than the authors suggest. The resolution should be increased or at least the choice of such a coarse resolution needs a very strong justification and discussion.

AAR: We address the above concern by taking the following steps: 1) providing a clearer explanation behind the choice of state vector resolution, and 2) including explicit statements in the revised manuscript that reflect our reasoning and providing discussion.

Our choice to use a state-level state vector encompassing 36 regions is motivated by the need to maintain a well-posed analytical inversion, especially considering the fidelity of the transport operator and the optimization strategy. In this study, we aim to minimize overfitting and instability while addressing (1) model errors (e.g. those resulting transport, prior, and representations) that are not well understood in this region, unlike in more data-rich areas, and (2) the heterogeneous observational coverage across the domain. Currently, the errors have not been sufficiently characterized due to a lack of sufficient *in situ* or TCCON-like observations in this region. While observations are utilized at ~10 km, the inversion control vector is set intentionally to a lower dimension. This "fine observation operator + coarse control vector" design is widely recommended in atmospheric methane inversions, where the design relies on several factors, such as transport model, prior flux representations, error characterization and the use of independent observations for evaluation.

Sicsik-Paré et al. (2025), the study suggested by the reviewer, performs European (region involving data-rich settings) inversions with a fixed state-vector dimension of 0.5°× 0.5° resolution, whereas the present study adopts a variable dimension corresponding to the political state, with the highest resolution not greater than ~0.6°. We acknowledge that the resolution of the retrieved state vectors is a limitation of this study, but this choice arises from the region being undersampled and understudied, as well as the need to address the likelihood of overly confident flux retrievals. To retrieve the maximum information content from TROPOMI without compromising the accuracy of the retrieved fluxes, further improvements in the demonstrated inversion strategy are required. This includes adequate characterization of both forward model and observational errors against independent observations, as well as conducting sensitivity tests to examine the representativeness of observations to retrieved fluxes. The above tasks thus warrant increased observational coverage and advanced inverse modeling techniques that properly account for such errors and sensitivities, which are currently limited over the region. With the advancement in observational coverage, future research can explore and evaluate different inverse techniques, such as the ensemble Kalman filter (EnKF) and 4D variational

inversion (4D-Var), that can handle highly resolved state vectors, leading to improved emissions at much finer scales.

The manuscript text is revised accordingly:

Revised Lines: 501-512 are as follows:

"We also acknowledge that the resolution of the retrieved emissions (as defined by state vectors) is a limitation when considering the information content that can be deduced from TROPOMI observations. For instance, Sicsik-Paré et al. (2025) demonstrated inversions over Europe using TROPOMI observations to retrieve fluxes at 0.5° × 0.5° resolution. The above-mentioned limitation of the present study stems from the region being undersampled and understudied against independent observations, as well as the need to address the risk of inferring overly confident flux retrievals. To retrieve the maximum information content from TROPOMI observations without compromising the accuracy of the retrieved fluxes, further improvements in the demonstrated inversion strategy are required. This includes adequate characterization of both forward model and observational errors against independent observations, as well as conducting sensitivity tests to examine the representativeness of observations to retrieve high-resolution fluxes. The above tasks thus warrant increased observational coverage and advanced inverse modeling techniques that properly account for such errors and sensitivities, which are currently limited over the region, not addressed in the study; thus, demand a future investigation in this direction."

Revised Lines: 563-568 are as follows:

"We emphasize the critical need for robust reporting of CH_4 emissions from the Indian region in global emission inventories. Achieving this requires an enhanced network of ground-based atmospheric trace gas measurements and advancements in satellite capabilities, alongside advanced modeling techniques with adequate model error characterisations. With the above expansion, future research can decisively explore and evaluate various inverse techniques. By implementing methods such as the Ensemble Kalman Filter (EnKF) and 4D Variational Inversion (4D-Var), we can effectively manage highly resolved state vectors, leading to significantly improved emissions data at much finer scales over India."

RC: 7. Non-inclusion of alternative TROPOMI/CAMS products and wetland optimization. The authors reject sensitivity tests with additional TROPOMI products, CAMS products, and wetland emissions on the grounds that differences between datasets are "within 16 ppb", the assumed observation uncertainty. This is not a convincing argument. Systematic differences between products, particularly in spatial patterns and bias structures, can influence posterior emissions even if pointwise differences are smaller than the nominal uncertainty. Recent studies (e.g. https://egusphere.copernicus.org/preprints/2025/egusphere2025-2622/) show large discrepancies

among the TROPOMI products. At minimum, the product differences and their potential impact must be discussed more rigorously.

AAR: The revised submission includes a discussion of systematic differences among satellite products and their potential impact on posterior uncertainties.

Regarding TROPOMI products: We examined three TROPOMI XCH_4 products (scientific, operational, and GOSAT-blended), and the results are included (new figures: Fig(s). 11, S14-16). Based on the systematic observational discrepancies found, we discuss the potential impacts on the inverse estimates (see the manuscript revision below).

We acknowledge that the credibility of satellite-based inversions also relies on the accuracy and sampling of XCH_4 products, and differences among them in terms of systematic biases and sampling may affect estimates considerably, especially at finer scales (e.g., *Sicsik-Paré et al.*, *2025).* To verify this in our case, a detailed performance assessment of different observational products is required, covering systematic retrieval errors, spatial and temporal coverage, and sampling inconsistencies. This demands extensive additional analyses involving multiple sensitivity tests using high-resolution inverse optimization altering the products, which warrant an independent future study but are beyond the scope of this study. Nevertheless, we emphasize the necessity to investigate the robustness of satellite-based inversions considering these differences. This focused approach will thus pave the way for more consistent emission estimates.

However, within the limit of the current inversion strategy, we performed an additional sensitivity experiment designed to test the impact of product differences in the midst of other unresolved modeling errors on posterior emission uncertainties. Specifically, we performed a separate inversion in which the measurement uncertainty was inflated (more than 50% relative to the baseline configuration) to consider differences among the TROPOMI XCH_4 products across the study region. The results suggest that the national-scale posterior uncertainty increases from 3.5 Tg yr^{-1} to 4.4 Tg yr^{-1}, indicating the possible influence of differences in multiple observational products on national-scale estimates. However, the above analysis does not take into account the spatial coverage differences between products as seen Fig. (s) S14 and S15 that may potentially affect the inverse estimates, and an assessment of such impacts requires further study as mentioned above.

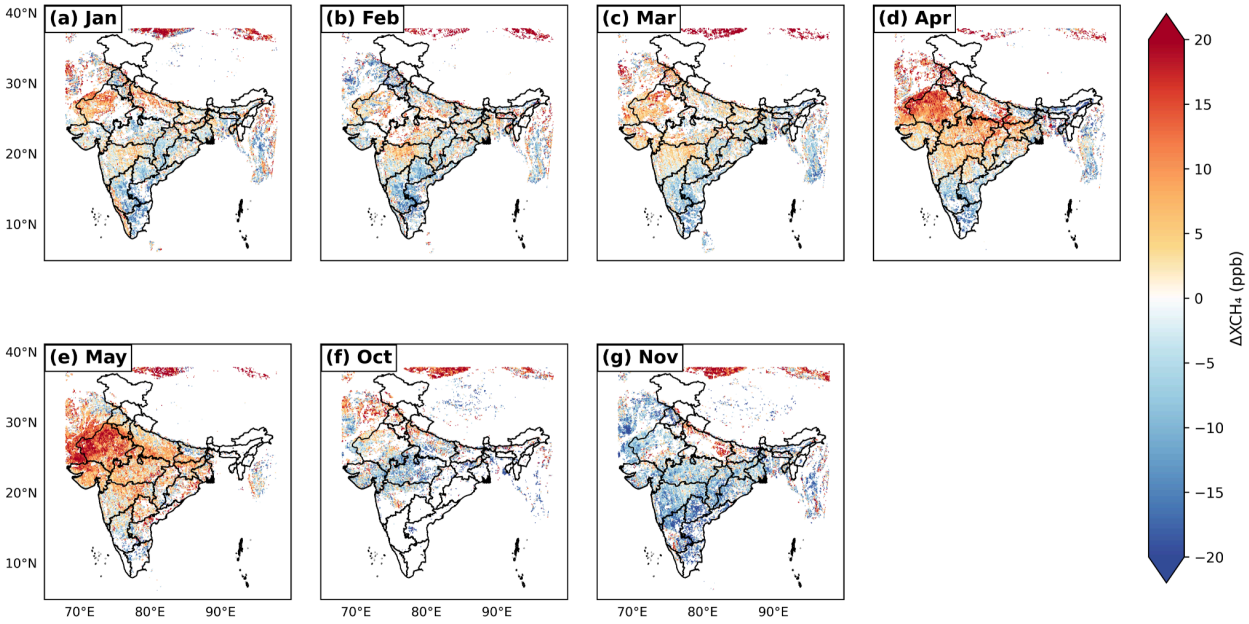

Figure 11: Spatial distribution of the difference between TROPOMI retrievals of XCH_4 (WFMD - Operational) for different months of 2019. Some months are omitted due to poor data coverage caused by filtering based on cloud pixels.

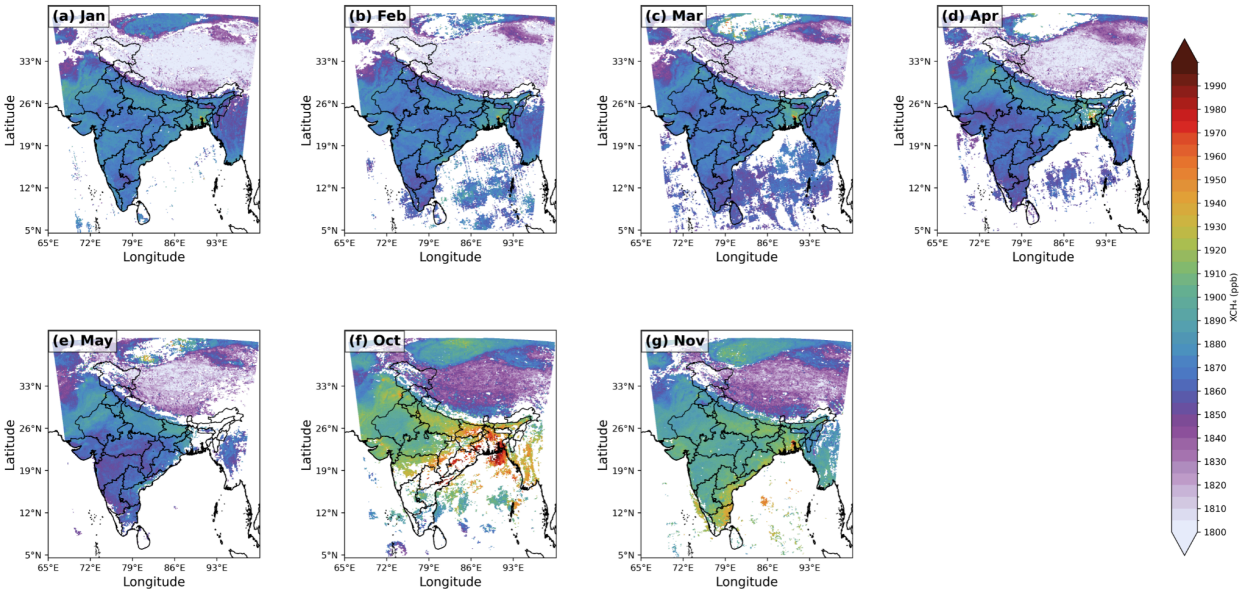

Figure S14: Spatial distribution of the TROPOMI (WFMD) retrievals of XCH_4 for different months of 2019. Some months are omitted due to poor data coverage caused by filtering based on cloud pixels.

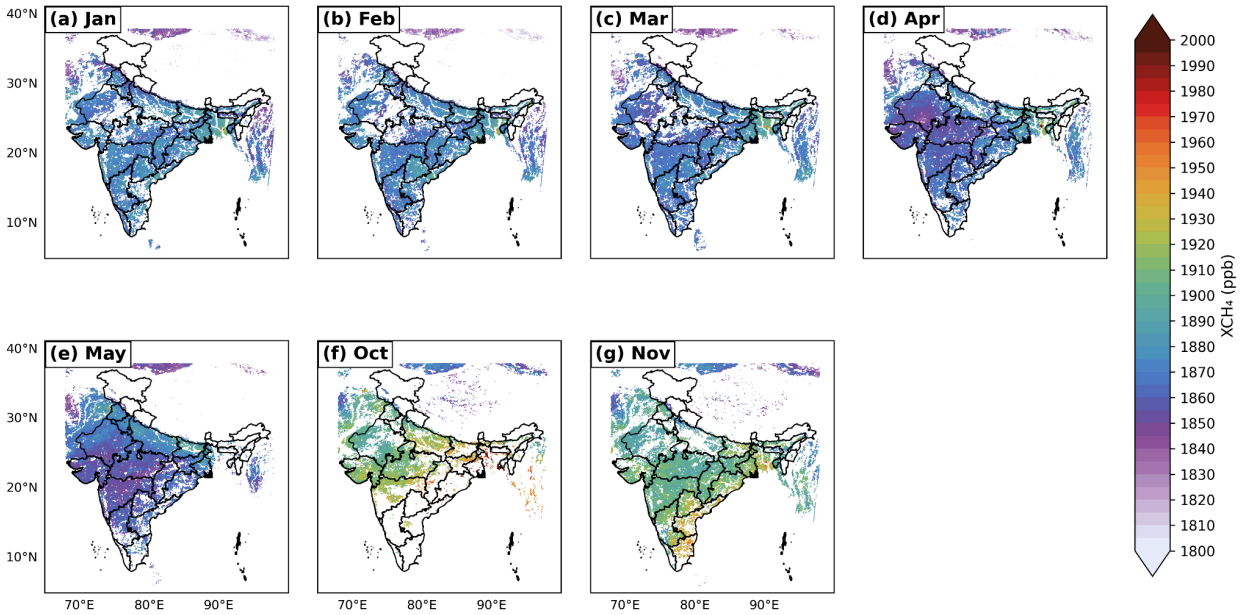

Figure S15: Spatial distribution of the TROPOMI (Operational) retrievals of XCH_4 for different months of 2019. Some months are omitted due to poor data coverage caused by filtering based on cloud pixels.

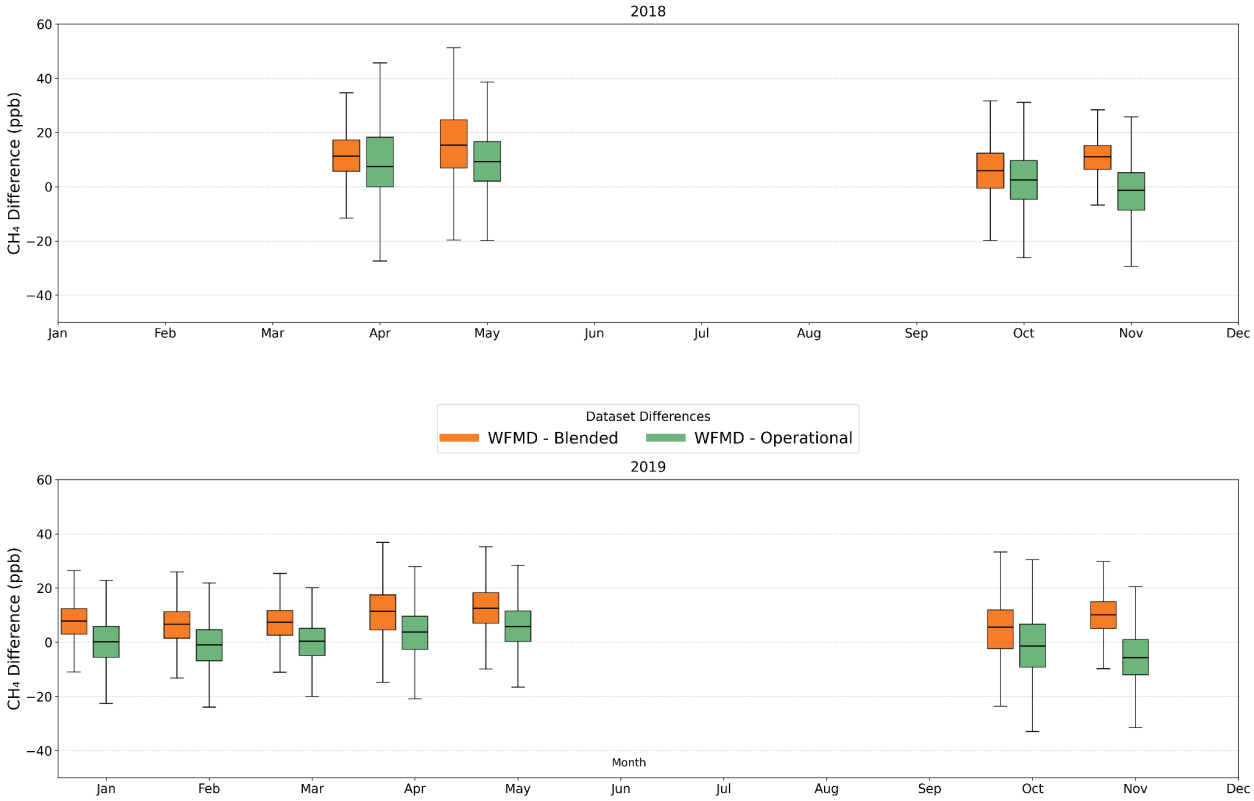

Figure S16. Differences between TROPOMI XCH_4 products (WFMD - blended and WFMD - Operational).

The manuscript is revised accordingly:

Revised Lines: 242-247 are as follows:

"Since multiple observational products are available and we may expect differences among those products, we assess product differences across our region using scientific, operational, and GOSAT-blended products. The additional data products are: the operational Sentinel-5P/TROPOMI Level-2 methane product provided by ESA/Copernicus (Copernicus Sentinel-5P, 2021), and the blended TROPOMI+GOSAT methane product available from April 2018 (Balasus et al., 2023). Further, we conduct an additional inversion by inflating the measurement uncertainty by more than 50 % (~25 ppb) to examine the influence of product differences on posterior flux uncertainties."

Revised Lines: 476-495 are as follows:

"We analyzed three TROPOMI XCH_4 products: scientific/WFMD (Schneising et al., 2023), operational (Copernicus Sentinel-5P, 2021), and GOSAT-blended (Balasus et al., 2023). The results are presented in Figs. 11 and S14-16. The above product comparison indicates that mean differences among these datasets over the region lie mostly in the range of 3 to 6 ppb at the monthly scale. Fig. 11 also indicates smaller spatial differences among these products across the Indian region. While these differences do not exceed the unresolved modeling errors, they can still influence inverse estimates, especially when fluxes are retrieved at finer scales. In our inverse setup as well, differences in the products can introduce additional uncertainty into estimates. For instance, using the increased measurement uncertainty as explained in Sect. 2.4.1, we find that the national-scale posterior uncertainty for 2018 increases from 3.5 Tg yr^{-1} in the baseline inversion to 4.4 Tg yr^{-1}. While the mean posterior emission estimates remained unchanged in our case, an increase in posterior uncertainty underscores the importance of addressing differences in satellite retrievals and their error characterization in inverse modeling.

While these mean differences are small across the region, the comparisons indicate considerable variation in spatial coverage between WFMD and Operational data products. For instance, Fig. S15 shows the spatial patterns of XCH_4 using the Operational product, but with comparatively sparse spatial coverage compared to those using the WFMD product (Fig. S14). Our analysis does not account for differences in spatial coverage between products, as illustrated in Figures S14 and S15. These differences may potentially affect the inverse estimates, and assessing their impact requires further study. A recent study also reveals considerable impacts of differences in retrievals on the inverse-based European CH_4 emission estimates when utilizing those TROPOMI XCH_4 products (Sicsik-Paré et al. 2025). While a detailed performance assessment of different observational products -regarding their coverage, retrieval errors, and spatial inconsistencies- is beyond the scope of this study, we emphasize the necessity to investigate the robustness of satellite-based inversions considering these differences, particularly at a finer scale. This focused approach will thus pave the way for more consistent emission estimates."

Revised Lines in Conclusion (Lines 568-572):

"Additionally, we recommend inter-comparisons of TROPOMI-based inversions using various inversion frameworks and transport models over India, with the aim of identifying biases in the forward models and the inversion frameworks. Further, we encourage rigorous sensitivity testing with TROPOMI inversions to assess the robustness of derived emissions, particularly with respect to differences in satellite products, coverage and sampling, as these factors can significantly influence inverse-based estimates."

Regarding the choice of the CAMS product for background representation:

We examined the CAMS Global Greenhouse Gas Reanalysis (EGG4), which has now been updated in Table 1, and compared it with the inverse-optimised CAMS product. Our analysis shows that the differences between these two datasets over India are within approximately 13 ppb (Fig. S8). After the spinup period, the variability in the simulated mole fractions is expected to be dominated by the local fluxes transported by the transport model, and any error is more likely due to errors in the transport model and local flux representations. It is anticipated that the differences in the tracer initial fields will converge during the spinup period, with the model simulations influenced by only a small fraction (less than 10 to 15 %) of their initial differences (e.g. Monteil et al., 2011). Further, conducting sensitivity tests using a different product for model initialisation and lateral boundary conditions would require repeating the entire transport model runs. Such analyses informing the potential impact of various tracer initializations on model simulations over this region thus demand a detailed future study dedicated to those aspects.

The manuscript is revised accordingly.

Revised Lines: 363-370 are as follows:

"Although we found that local fluxes had a more dominant contribution to the observed variability than the background contributions (see Fig. S7), there can be non-negligible differences arising from the choice of global model products used for initialization. For instance, we conducted additional analysis comparing the CAMS EGG4 product, which was used for initialization in this study, with the inverse-optimized CAMS product (Bergamaschi et al., 2013). This comparison indicated a difference of approximately 13 ppb over India (see Fig. S8). While it is expected that only a small fraction (less than 10 to 15 %) of these initial tracer differences will effectively converge to influence model simulations after the spinup period (e.g. Monteil et al., 2011), the potential impact of various tracer initializations on model simulations over this region is not addressed in the current study. The above aspect is worth a future investigation through a dedicated model sensitivity study."

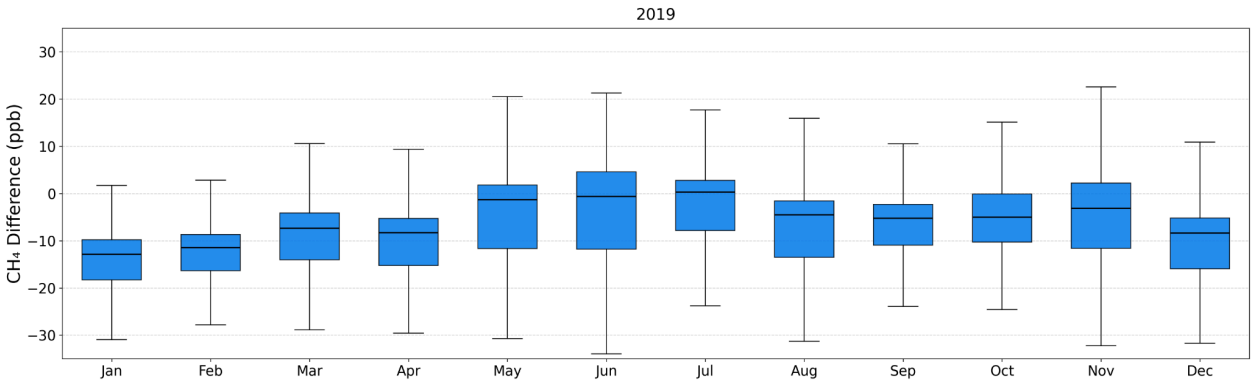

Figure S8: Difference in CAMS EEG4 (reanalysis) and the latest version (data not available for 2018) of inversion optimised dataset (using satellite+ surface-air sampled data) for 2019.

Regarding wetland emissions:

The present analysis excluded wetland emissions from the optimization because the modeled XCH_4 enhancements over India associated with wetlands are significantly smaller (0.5 to 0.9 ppb) than the anthropogenic enhancements, and the ratio of mixing ratio enhancements shows a negligible impact from wetlands (see Fig(s). S9 and S10). As a result, wetland emissions are excluded from our inverse analysis.

The manuscript is revised accordingly:

Revised Lines: 513-515 are as follows:

"The present analysis excluded wetland emissions from the optimization due to their negligible contribution to column enhancements. This is demonstrated in Figs. S9 and S10, which show that the simulated wetland emission enhancements in the column are significantly smaller than anthropogenic enhancements."

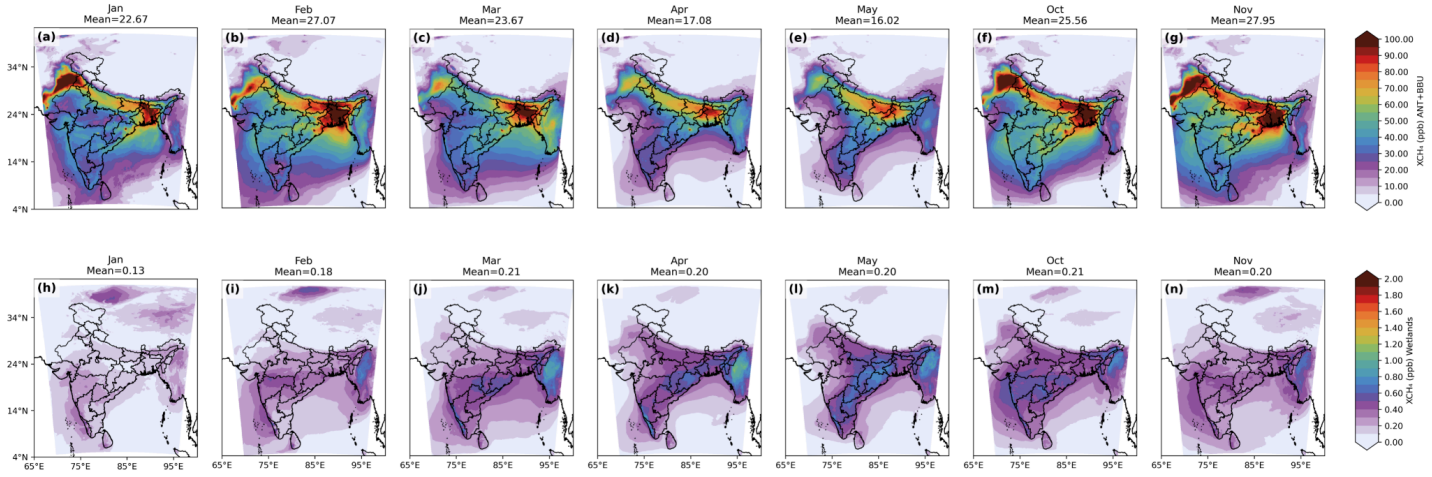

Figure S9: Spatial distribution for WRF-GHG simulated XCH_4 from (a)-(g) anthropogenic + biomass burning and (h)-(n) wetland sources for different months of 2018. The months omitted in Fig. 7 are excluded here as well.

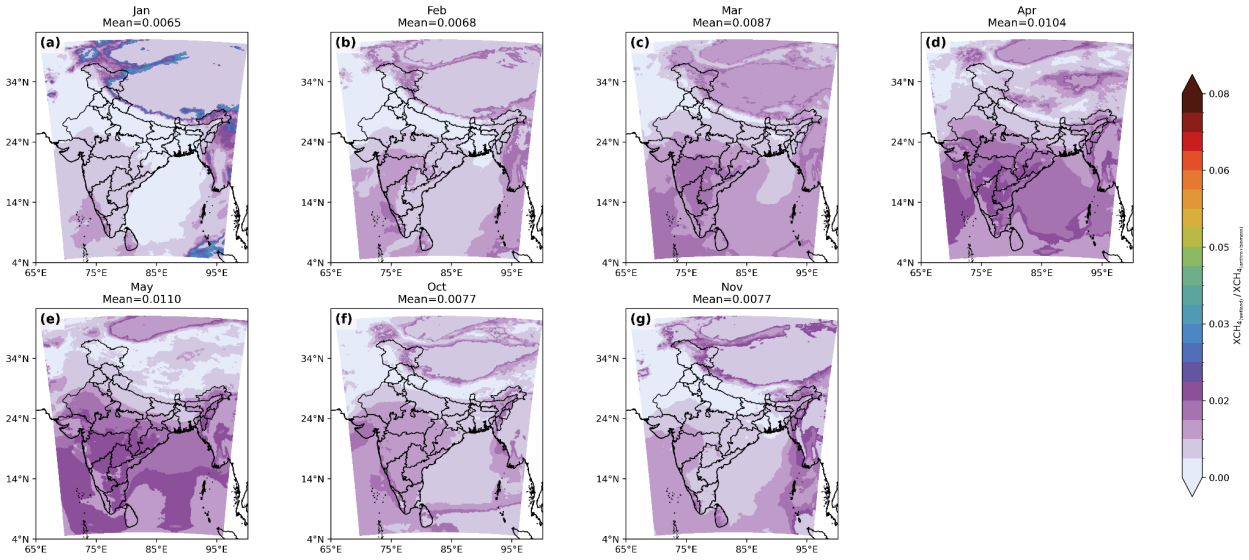

Figure S10: The ratio of simulated XCH_4 contributed from wetland to that from anthropogenic and biomass burning sources (i.e. $XCH_{4\,(wetland)}/XCH_{4(anthro+biomass)}$ for different months of 2018. The months that are omitted in Fig. 7 are excluded here as well.

RC: 8. Inconsistent description of emission sources in the Introduction. Line 43 states that enteric fermentation accounts for 8% of India's total GHG emissions, while Figure 2 shows a contribution of 42%. This is confusing. It would be clearer to express contributions relative to total CH_4 emissions, not total GHG emissions. This discrepancy should be corrected for clarity

AAR: Done
Revised Lines: 42 are as follows
"CH_4 emissions from enteric fermentation account for about 44 % of the total CH_4 emissions of India's National GHG inventory 2020 (MoEFCC, 2024)."

RC: 9. Unclear whether one or two inversions were performed. It is not clear whether the authors conducted one inversion (including both anthropogenic and biomass-burning fluxes) or two separate inversions for EDGAR and EDGAR+GFAS. This needs to be stated explicitly. Please clarify how many inversions were performed and how the components were treated.

AAR: Done. The manuscript is revised accordingly:

Revised Lines: 433-437 are as follows:

"In this section, we present estimates of India's anthropogenic CH_4 budget for the period 2018–2019 derived through inverse optimization as described in Sect. 3.2. Two separate inversions were performed using identical model configurations and observational constraints: one including biomass-burning emissions from GFAS in addition to anthropogenic sources, and another excluding biomass-burning emissions. Posterior emission estimates from both inversions are reported separately to quantify the impact of biomass burning on inferred anthropogenic CH_4 emissions."

References:

1. Agustí-Panareda, A., Barré, J., Massart, S., Inness, A., Aben, I., Ades, M., Baier, B. C., Balsamo, G., Borsdorff, T., Bousserez, N., Boussetta, S., Buchwitz, M., Cantarello, L., Crevoisier, C., Engelen, R., Eskes, H., Flemming, J., Garrigues, S., Hasekamp, O., Huijnen, V., Jones, L., Kipling, Z., Langerock, B., McNorton, J., Meilhac, N., Noël, S., Parrington, M., Peuch, V.-H., Ramonet, M., Razinger, M., Reuter, M., Ribas, R., Suttie, M., Sweeney, C., Tarniewicz, J., and Wu, L.: Technical note: The CAMS greenhouse gas reanalysis from 2003 to 2020, Atmospheric Chemistry and Physics, 23, 3829–3859, https://doi.org/10.5194/acp-23-3829-2023, 2023.
2. Bergamaschi, Peter, Sander Houweling, Arjo Segers, Maarten Krol, Christian Frankenberg, R. A. Scheepmaker, Edward Dlugokencky et al. "Atmospheric CH4 in the first decade of the 21st century: Inverse modeling analysis using SCIAMACHY satellite retrievals and NOAA surface measurements." *Journal of Geophysical Research: Atmospheres* 118, no. 13 (2013): 7350-7369.
3. Bisht, J. S. H., Patra, P. K., Takigawa, M., Sekiya, T., Kanaya, Y., Saitoh, N., and Miyazaki, K.: Estimation of CH44 emission based on an advanced 4D-LETKF assimilation system, Geosci. Model Dev., 16, 1823–1838, https://doi.org/10.5194/gmd-16-1823-2023, 2023.
4. Balasus, N., Jacob, D. J., Lorente, A., Maasakkers, J. D., Parker, R. J., Boesch, H., Chen, Z., Kelp, M. M., Nesser, H., and Varon, D. J.: A blended TROPOMI+GOSAT satellite data product for atmospheric methane using machine learning to correct retrieval biases, Atmospheric Measurement Techniques, 16, 3787–3807, https://doi.org/10.5194/amt-16-3787-2023, 2023.
5. Brasseur, G. P. and Jacob, D. J.: Modeling of Atmospheric Chemistry, Cambridge University Press, Cambridge, https://doi.org/10.1017/9781316544754, 2017.

6. Broquet, G., Bréon, F.-M., Renault, E., Buchwitz, M., Reuter, M., Bovensmann, H., Chevallier, F., Wu, L., and Ciais, P.: The potential of satellite spectro-imagery for monitoring CO2 emissions from large cities, Atmos. Meas. Tech., 11, 681–708, https://doi.org/10.5194/amt-11-681-2018, 2018.
7. Bruch, V., Rösch, T., Jiménez de la Cuesta Otero, D., Ellerhoff, B., Mamtimin, B., Becker, N., Blechschmidt, A.-M., Förstner, J., and Kaiser-Weiss, A. K.: German methane fluxes estimated top-down using ICON–ART – Part 1: Ensemble-enhanced scaling inversion, *Atmos. Chem. Phys.*, 25, 17159–17185, https://doi.org/10.5194/acp-25-17159-2025, 2025.
8. Callewaert, S., Zhou, M., Langerock, B., Wang, P., Wang, T., Mahieu, E., and De Mazière, M.: A WRF-Chem study of the greenhouse gas column and in situ surface concentrations observed in Xianghe, China – Part 1: Methane (CH4), Atmospheric Chemistry and Physics, 25, 9519–9544, https://doi.org/10.5194/acp-25-9519-2025, 2025.
9. Copernicus Sentinel-5P (processed by ESA), 2021, TROPOMI Level 2 Methane Total Column products. Version 02. European Space Agency. https://doi.org/10.5270/S5P-3lcdqiv
10. East, James D., Daniel J. Jacob, Dylan Jervis, Nicholas Balasus, Lucas A. Estrada, Sarah E. Hancock, Melissa P. Sulprizio et al. "Worldwide inference of national methane emissions by inversion of satellite observations with UNFCCC prior estimates." *Nature Communications* 16, no. 1 (2025): 11004.
11. Estrada, L. A., Varon, D. J., Sulprizio, M., Nesser, H., Chen, Z., Balasus, N., ... & Jacob, D. J. (2025). Integrated Methane Inversion (IMI) 2.0: an improved research and stakeholder tool for monitoring total methane emissions with high resolution worldwide using TROPOMI satellite observations. *Geoscientific Model Development*, *18*(11), 3311-3330.
12. Hancock, S. E., Jacob, D. J., Chen, Z., Nesser, H., Davitt, A., Varon, D. J., Sulprizio, M. P., Balasus, N., Estrada, L. A., Cazorla, M., Dawidowski, L., Diez, S., East, J. D., Penn, E., Randles, C. A., Worden, J., Aben, I., Parker, R. J., and Maasakkers, J. D.: Satellite quantification of methane emissions from South American countries: a high-resolution inversion of TROPOMI and GOSAT observations, Atmos. Chem. Phys., 25, 797–817, https://doi.org/10.5194/acp-25-797-2025, 2025.

13. Kuhlmann, G., Brunner, D., Broquet, G., and Meijer, Y.: Quantifying CO2 emissions of a city with the Copernicus Anthropogenic CO2 Monitoring satellite mission, Atmos. Meas. Tech., 13, 6733–6754, https://doi.org/10.5194/amt-13-6733-2020, 2020.
14. Kumar, P., Broquet, G., Caldow, C., Laurent, O., Gichuki, S., Cropley, F., Yver-Kwok, C., Fontanier, B., Lauvaux, T., Ramonet, M., Shah, A., Berthe, G., Martin, F., Duclaux, O., Juery, C., Bouchet, C., Pitt, J., and Ciais, P.: Near-field atmospheric inversions for the localization and quantification of controlled methane releases using stationary and mobile measurements, *Q. J. Roy. Meteor. Soc.*, 148, 1886–1912, https://doi.org/10.1002/qj.4283, 2022.
15. Lu, Xiao, Daniel J. Jacob, Yuzhong Zhang, Joannes D. Maasakkers, Melissa P. Sulprizio, Lu Shen, Zhen Qu et al. "Global methane budget and trend, 2010–2017: complementarity of inverse analyses using in situ (GLOBALVIEWplus CH 4 ObsPack) and satellite (GOSAT) observations." *Atmospheric Chemistry and Physics* 21, no. 6 (2021): 4637-4657.
16. Monteil, G., Houweling, S., Dlugockenky, E., Maenhout, G., Vaughn, B., White, J., and Rockmann, T.: Interpreting methane variations in the past two decades using measurements of CH4 mixing ratio and isotopic composition, Atmospheric Chemistry and Physics, 11,9141–9153, 2011.
17. Pendergrass, D. C., Jacob, D. J., Balasus, N., Estrada, L., Varon, D. J., East, J. D., Mooring, T. A., Penn, E., Nesser, H., and Worden, J. R.: Trends and seasonality of 2019–2023 global methane emissions inferred from a localized ensemble transform Kalman filter (CHEEREIO v1.3.1) applied to TROPOMI satellite observations, Atmos. Chem. Phys., 25, 14353–14369, https://doi.org/10.5194/acp-25-14353-2025, 2025.
18. Pillai, D., Buchwitz, M., Gerbig, C., Koch, T., Reuter, M., Bovensmann, H., Marshall, J., and Burrows, J. P.: Tracking city CO2 emissions from space using a high-resolution inverse modelling approach: a case study for Berlin, Germany, Atmos. Chem. Phys., 16, 9591–9610, https://doi.org/10.5194/acp-16-9591-2016, 2016.
19. Qu, Z., Jacob, D.J., Shen, L., Lu, X., Zhang, Y., Scarpelli, T.R., Nesser, H., Sulprizio, M.P., Maasakkers, J.D., Bloom, A.A. and Worden, J.R., 2021. Global distribution of methane emissions: a comparative inverse analysis of observations from the TROPOMI

and GOSAT satellite instruments. *Atmospheric Chemistry and Physics*, *21*(18), pp.14159-14175.

20. Saunois M, Stavert AR, Poulter B, Bousquet P, Canadell JG, Jackson RB, Raymond PA, Dlugokencky EJ, Houweling S, Patra PK, Ciais P. The global methane budget 2000–2017. Earth System Science Data Discussions. 2019 Aug 19;2019:1-36.
21. Scarpelli, T.R., Jacob, D.J., Grossman, S., Lu, X., Qu, Z., Sulprizio, M.P., Zhang, Y., Reuland, F., Gordon, D. and Worden, J.R., 2022. Updated Global Fuel Exploitation Inventory (GFEI) for methane emissions from the oil, gas, and coal sectors: evaluation with inversions of atmospheric methane observations. *Atmospheric Chemistry and Physics*, *22*(5), pp.3235-3249.
22. Shen, L., Jacob, D.J., Gautam, R., Omara, M., Scarpelli, T.R., Lorente, A., Zavala-Araiza, D., Lu, X., Chen, Z. and Lin, J., 2023. National quantifications of methane emissions from fuel exploitation using high resolution inversions of satellite observations. *Nature Communications*, *14*(1), p.4948.
23. Schneising, O., Buchwitz, M., Hachmeister, J., Vanselow, S., Reuter, M., Buschmann, M., Bovensmann, H., and Burrows, J. P.: Advances in retrieving XCH4 and XCO from Sentinel-5 Precursor: improvements in the scientific TROPOMI/WFMD algorithm, Atmos. Meas. Tech., 16, 669–694, https://doi.org/10.5194/amt-16-669-2023, 2023.
24. Sicsik-Paré, A., Fortems-Cheiney, A., Pison, I., Broquet, G., Opler, A., Potier, E., Martinez, A., Schneising, O., Buchwitz, M., Maasakkers, J. D., et al.: Can we obtain consistent estimates of the emissions in Europe from three different CH 4 TROPOMI products?, EGUsphere, 2025, 1–48, 2025.
25. Stevenson, D. S., Zhao, A., Naik, V., O'Connor, F. M., Tilmes, S., Zeng, G., Murray, L. T., Collins, W. J., Griffiths, P. T., Shim, S., Horowitz, L. W., Sentman, L. T., and Emmons, L.: Trends in global tropospheric hydroxyl radical and methane lifetime since 1850 from AerChemMIP, Atmos. Chem. Phys., 20, 12905–12920, https://doi.org/10.5194/acp-20-12905-2020, 2020.
26. Turner, A.J., Jacob, D.J., Wecht, K.J., Maasakkers, J.D., Lundgren, E., Andrews, A.E., Biraud, S.C., Boesch, H., Bowman, K.W., Deutscher, N.M. and Dubey, M.K., 2015. Estimating global and North American methane emissions with high spatial resolution using GOSAT satellite data. *Atmospheric Chemistry and Physics*, *15*(12), pp.7049-7069.

27. Wang, Y., Yuan, Q., Li, T., Yang, Y., Zhou, S., and Zhang, L.: Seamless mapping of long-term (2010–2020) daily global XCO2 and XCH4 from the Greenhouse Gases Observing Satellite (GOSAT), Orbiting Carbon Observatory 2 (OCO-2), and CAMS global green-house gas reanalysis (CAMS-EGG4) with a spatiotemporally self-supervised fusion method, Earth System Science Data, 15, 3597–3622, https://doi.org/10.5194/essd-15-3597-2023, 2023.
28. Wang, Z., Warneke, T., Deutscher, N. M., Notholt, J., Karstens, U., Saunois, M., Schneider, M., Sussmann, R., Sembhi, H., Griffith, D. W. T.,Pollard, D. F., Kivi, R., Petri, C., Velazco, V. A., Ramonet, M., and Chen, H.: Contributions of the troposphere and stratosphere to CH4 model biases, Atmospheric Chemistry and Physics, 17, 13 283–13 295, https://doi.org/10.5194/acp-17-13283-2017, 2017.
29. Ye, Xinxin, Thomas Lauvaux, Eric A. Kort, Tomohiro Oda, Sha Feng, John C. Lin, Emily G. Yang, and Dien Wu. "Constraining fossil fuel CO2 emissions from urban area using OCO‐2 observations of total column CO2." *Journal of Geophysical Research: Atmospheres* 125, no. 8 (2020): e2019JD030528.